Journal of Materials Chemistry B

Accepted Manuscript

ROYAL SOCIETY OF CHEMISTRY

www.rsc.org/materialsB

Journal of Materials Chemistry B RSCPublishing

ARTICLE

A Graphene Oxide/Conducting Polymer Nanocomposite for Electrochemical Dopamine Detection: Origin of Improved Sensitivity and Specificity

Cite this: DOI: 10.1039/x0xx00000x

Received 00th January 2012,
Accepted 00th January 2012

DOI: 10.1039/x0xx00000x

www.rsc.org/

C.L. Weaver,[a,b,c] H. Li[a], X. Luo[d] and X.T. Cui[a,b,c]

Neuromodulatory dopamine (DA) acts as an essential signaling molecule in the central nervous system (CNS), and its dysfunction has been implicated in neurological disorders such as Parkinson's disease and schizophrenia. Due to its inherent redox properties, DA can be detected electrochemically by monitoring changes in current as the molecule is oxidized. Many electrode materials for electrochemical detection have been developed to monitor DA, but properties such as sensitivity and specificity must be optimized. We describe a conducting polymer (CP) nanocomposite of poly(3,4-ethylendioxythiophene) (PEDOT) doped with GO nanosheets, and report its superior DA detection performance over bare glassy carbon electrode (GCE) substrates. The GO/PEDOT electrode exhibits favorable electrical properties such as lowered impedance and increased charge storage capacity. The nanocomposite demonstrates improved sensitivity to the oxidation of DA at its surface. Meanwhile, interference from competing analyte, ascorbic acid (AA), is minimized. Mechanistic studies indicate that electrostatic interactions drive the increased sensitivity toward DA, and improved electrocatalysis of AA oxidation by the nanocomposite enables the selective discrimination of DA signals from those of AA. The described performance of the GO/PEDOT nanocomposite accentuates its promise for improving detection capabilities of electrochemical biosensors for the accurate and reliable detection of DA signals in biological samples.

1. Introduction

Efforts toward the development of detection methods that allow sensitive real-time monitoring of neurotransmitter signaling within the central nervous system (CNS), or point of care sampling from blood, urine or cerebrospinal fluid (CSF), have received increasing attention in recent years. The signaling of one such neurotransmitter, dopamine (DA), within the CNS orchestrates many behaviors such as learning, motivation, and motor control [1], and its dysfunction has been implicated in multiple diseases such as Parkinson's [2], schizophrenia [3], and addiction [4]. Additionally, DA has been investigated as a peripheral biomarker for the diagnosis of Parkinson's disease [5] and adrenal tumors [6]. The potential of utilizing DA signaling for both diagnostic and basic science applications motivates the development of low-cost tools for monitoring catecholamine levels in biological fluids and tissue [7,8].

Traditional methods of DA detection of biological fluids include chromatography analysis, colorimetric detection, and spectroscopic analysis, among others [9-11]. These methods require complicated, expensive equipment or reagents, and have long sample processing times that impede their use by clinicians and makes exploratory research slow and costly. Electrochemical methods of detection have been developed that take advantage of the redox activity of DA molecules and enable simple, rapid analysis of biological samples using low-cost electrodes as sensors [8]. However, current electrochemical sensors suffer from limited sensitivity and specificity towards DA [12]. Physiological levels of DA range from nanomolar to low micromolar, creating a need for highly sensitive tools with very low detection limits [8]. Furthermore, in biological samples that contain DA, there also exist a variety of interfering molecules, such as ascorbic acid (AA) and uric acid (UA), that exhibit similar redox behavior and can obscure DA signals [13-15].

To address the shortcomings in sensor sensitivity and specificity, researchers have developed a variety of electrode modifications to improve these properties. Conducting

polymers (CPs), such as poly(3,4-ethylenedioxythiophene) (PEDOT), polypyrrole and polyaniline, deposited on the surface of electrodes have improved sensor performance by increasing sensitivity and selectivity towards DA as a result of CP film properties such as hydrophobicity, charge, and large surface area [13, 15-17]. Additionally, the synthesis reaction of CP films enables simple incorporation of enzymes or nanomaterials to create customizable and highly sensitive sensor materials [17-20]. Graphene-based materials also have received much focus as biosensor materials because of their unique electrical and chemical properties [21-22]. Reduced graphene oxide (RGO), synthesized by the chemical or electrochemical reduction of graphene oxide (GO), exhibits rapid electron transfer kinetics that enables highly sensitive detection of DA [23-24], and composites of RGO with a variety of other materials have demonstrated the ability to selectively detect DA in the presence of interfering species [25-28]. However, little work has been done to characterize the potential of its precursor, GO, as a DA sensor. By itself, GO exhibits poor conductivity compared to its reduced form, requiring its incorporation into a conductive matrix in order to act as an effective electrode coating. CPs, such as PEDOT, have been utilized to create stable, conductive nanocomposites with GO, and have demonstrated potential for electrical recording and biointerfacing applications [29-34]. In this work, we describe a GO/PEDOT nanocomposite material and demonstrate that GO, in its unreduced form within a CP matrix, creates a sensitive and selective sensor for DA detection. The GO/PEDOT nanocomposite selectively amplifies the DA oxidation signal, but not AA or UA signals, as a result of electrostatic interactions between DA molecules and the nanocomposite surface. In addition, the nanocomposite reduces interference from AA as a result of a significant shift in its oxidation potential due to an electrocatalytic effect of the nanocomposite material on the AA oxidation reaction. The performance of the GO/PEDOT nanocomposite for selective and sensitive DA oxidation along with its electrochemical stability underlines the potential of the nanocomposite material as a novel electrode modification for the development of improved DA sensors.

2. Experimental Section

2.1 Materials

L-ascorbic acid (AA), 3,4-dihydroxyphenylacetic acid (DOPAC), 3,4-ethylenedioxythiophene (EDOT), 3-hydroxytyramine hydrochloride (DA), potassium chloride (KCl), sodium chloride (NaCl) and uric acid (UA) were purchased from Sigma-Aldrich. Monosodium phosphate and disodium phosphate were purchased from Fisher Scientific. Graphite powder (SP-1) was purchased from Bay Carbon, Incorporated. Phosphate buffed saline (PBS, 10x) was purchased from EMD Millipore and diluted to a 1X working concentration for all experiments (137 mM NaCl, 2.7 mM KCl, 10 mM phosphate buffer). Purified H_2O filtered through a Milli-Q System (EMD Millipore) was used throughout all experiments.

2.2 GO Synthesis

GO was synthesized as previously described using the modified Hummer's method, and stored in H_2O until use [33, 35]. Prior to deposition into the nanocomposite, GO nanosheets were mechanically exfoliated with a probe sonicator in H_2O for 15 min, 30 min, 60 min, or 90 min to alter the thickness and x-y size of the nanoparticles [33].

2.3 Electrochemical Apparatus

A Gamry potentiostat, FAS2 femtostat (Gamry Instruments) was used for electrode pretreatment, GO/PEDOT nanocomposite film polymerization and impedance measurements. An Autolab potentiostat/galvanostat PGSTAT128N was used for all analyte detection assays. All electrochemical experiments were carried out using a three-electrode setup consisting of a glassy carbon working electrode (GCE, 3 mm diameter, CH Instruments), a silver/silver chloride reference electrode (CH Instruments) and a platinum foil counter electrode.

2.4 Electropolymerization of GO/PEDOT Nanocomposite Film

GCEs were polished with 1.0 and 0.05 μm alumina slurries and cleaned by sonication in 100% ethanol followed by H_2O. The GCEs were electrochemically pretreated in PBS by applying a cleaning voltage pulse (-2 V, 250 s), followed by a cyclic voltammetry sweep (0.3 V to 1.3 V, 100 mV s^{-1}, 5 cycles). Following pretreatment, GO/PEDOT nanocomposite films were electrochemically deposited onto GCEs from a polymerization solution composed of EDOT (0.2 M) and GO (5 mg ml^{-1}). GO/PEDOT nanocomposite films were synthesized using GO nanosheets that had been sonicated for 15 min (GO15), 30 min (GO30), 60 min (GO60) or 90 min (GO90). An oxidizing current of 20 μA was applied through the GCE for 200 s to carry out the polymerization reaction. The GO/PEDOT modified GCEs were gently rinsed in H_2O to remove any adsorbed monomer or GO, and stored in H_2O until use.

2.5 Nanocomposite Characterization

GO/PEDOT nanocomposite surface morphology was imaged using a scanning electron microscope (SEM, JEOL JSM6510) with an operating potential of 3 kV. The atomic ratio of oxygen to sulfur was calculated as a semi-quantitative estimate of the amount of GO contained in the nanocomposite film. Elemental analysis was carried out using energy dispersive spectroscopy (EDS, Oxford INCA EDS) with an operating potential of 20 kV. For each sample (n = 4 per sonication group), the atomic percent of oxygen and sulfur were measured from three separate areas, and averaged to obtain the mean value for the sample.

The chemical bonds in the nanocomposite films were evaluated with attenuated total reflectance Fourier-transform infrared spectroscopy (ATR-FTIR) using a Bruker Vertex 70 spectrometer with a Hyperion 2000 microscope and 20x ATR objective. For each sample (n = 4 per sonication group), three

separate areas were analyzed, and all spectra were averaged to obtain one spectrum per group. The areas underneath the alkoxy C-O peak (1064 cm^{-1}) and the C-S peak (845 cm^{-1}) on the averaged spectra were calculated using custom MATLAB software to evaluate changes in relative alkoxy content with increasing GO sonication treatment.

Electrochemical impedance measurements were collected in PBS using an alternating current sinusoid of 10 mV. Electrochemical stability of the nanocomposite was characterized by collecting impedance measurements in the frequency range between 1 Hz and 100 kHz after 0, 2, and 1000 cyclic voltammetry (CV) sweeps from -0.5 V to 0.6 V at 100 mV s^{-1}. The electrochemical properties of the nanocomposite synthesized with GO treated for various sonication times were evaluated by collecting impedance measurements in the frequency range between 10 mHz and 100 kHz (n = 7 per sonication group).

2.6 Electrochemical Detection of DA, AA, UA, and DOPAC

All electrochemical detection assays were carried out in PBS using CV with a voltage sweep from -0.5 V to 0.6 V at a speed of 100 mV s^{-1}. Electrodes were immersed in the electrochemical cell, and known concentrations of DA, AA, UA or DOPAC were added to the PBS with a 30 s equilibration time prior to CV measurement. The oxidation peak location (Ep) was defined as the point at which the oxidation current reached its maximum. The oxidation peak current (Ip) was determined after a PBS background subtraction as the maximum current value of the oxidation peak. For assays carried out at a basic pH (9.5), PBS was prepared at the appropriate pH by altering the ratio of monosodium phosphate to disodium phosphate (3.2 mM monosodium phosphate, 2.67 M disodium phosphate), while maintaining the same phosphate buffer strength (10 mM) and ionic content (137 mM NaCl, 2.7 mM KCl) as the purchased pH 7.4 PBS. The limit of detection (LOD) was calculated as three times the standard deviation of the CV current response in PBS (n = 6).

2.7 Statistical Analysis

All statistical analyses were carried out in GraphPad Prism software. All data are presented as the mean ± standard error of the mean. Comparisons across two experimental groups were made with Student's t-test, and comparisons across greater than two experimental groups were made with one-way analysis of variance followed by Tukey's post hoc analysis. DA calibration curves were analyzed using linear regression. Calculated p-values of $p < 0.05$ were considered statistically significant.

3. Results and discussion

3.1 Stability and Electrochemical Properties of the GO/PEDOT Nanocomposite

GO/PEDOT nanocomposite films were electrodeposited onto bare GCE electrodes from an aqueous solution of monomer and GO nanosheets. During CP electrodeposition, oxidation of the monomer via electrical stimulation elicits free radical polymerization during which the polymer deposits onto the anode surface, incorporating negatively charged molecules from the polymerization solution as dopants in order to electrostatically balance positive charges formed on the polymer backbone. The GO nanosheets contain multiple negatively charged carboxylic acid groups on their edges, enabling their incorporation into the PEDOT film [31, 34]. The resulting film exhibits a morphology consisting of sub-micron, fuzzy, sheet-like features that are likely GO nanosheets

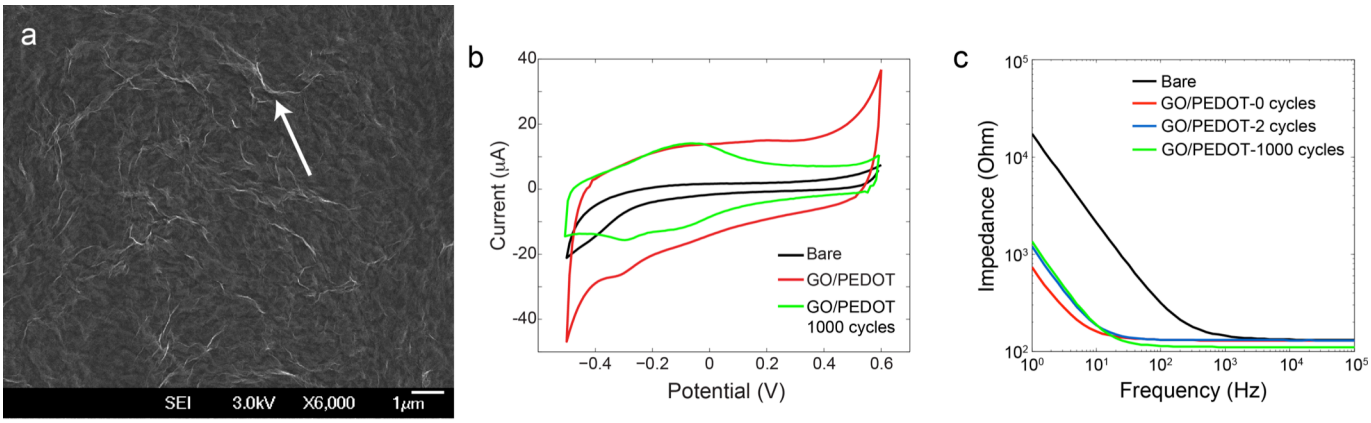

Figure 1. Characterization of the GO/PEDOT Nanocomposite Material. (a) Scanning electron micrograph of the GO/PEDOT nanocomposite illustrating its sheetlike morphology. The arrow points out a wrinkle feature that is likely due to the protrusion of a GO sheet from the polymer surface. (b) CV of a bare GC electrode and the GO/PEDOT-modified electrode in PBS (scan rate: 100 mV s^{-1}) demonstrating the increase in charge storage capacity after modification. (c) EIS of the bare GC electrode and the GO/PEDOT-modified electrodes after repeated CV cycling in PBS (-0.5 V to 0.6 V; 100 mV s^{-1}). The nanocomposite retains its stability after 1000 CV cycles.

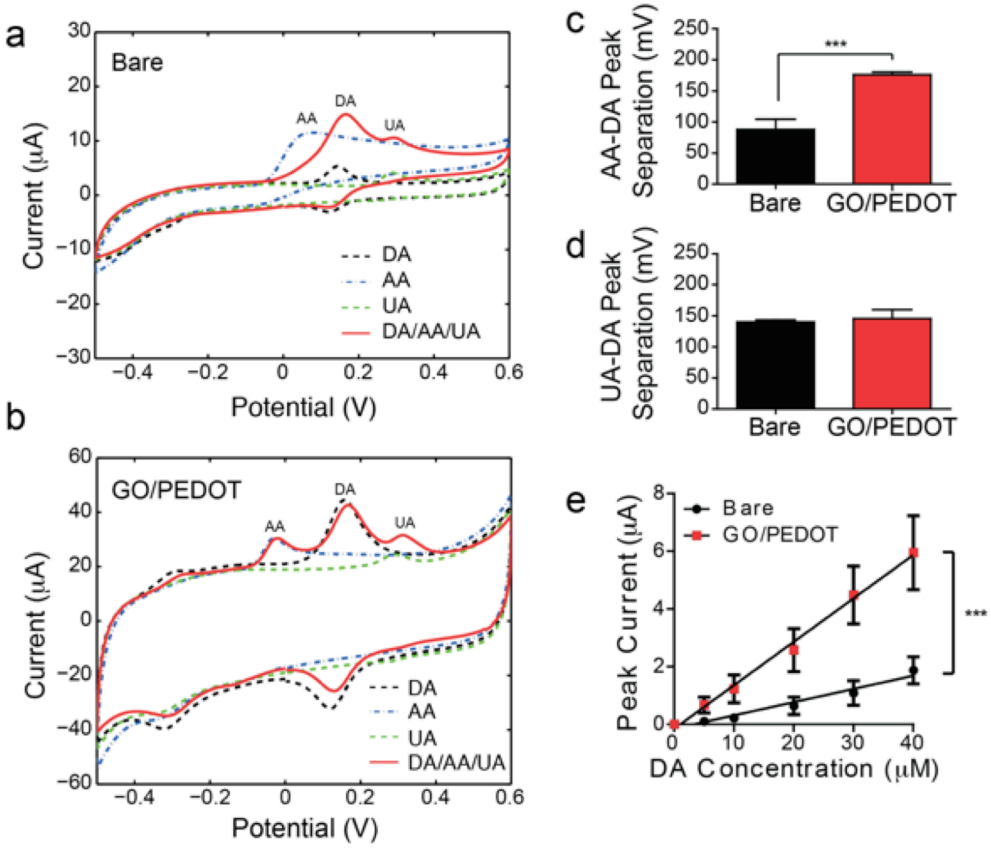

Figure 2: Electrochemical Oxidation of DA in the Presence of Interfering Species. CVs of the (a) bare GCE and (b) GO/PEDOT-modified electrode in solutions containing 100 μM DA, 1 mM AA, 100 μM UA alone or in combination. Three separate oxidation peaks are discernable on the GO/PEDOT-modified electrode, but not the bare GCE, in solutions containing all three analytes. Total separation between the (c) AA and DA oxidation peaks, and the (d) UA and DA oxidation peaks. There is a significant increase in separation between the AA and DA oxidation peaks at the GO/PEDOT nanocomposite (*** $p < 0.001$; $n = 7$). (e) Linear DA detection curves for the bare GC and GO/PEDOT-modified electrodes, illustrating the increased senstivity of the modified electrodes to DA (*** $p < 0.001$; $n = 7$).

engulfed in the PEDOT matrix (Figure 1a). The nanocomposite also contains sharp wrinkles that are characteristic of pure GO films and can be observed in CP films doped with GO [32, 36]. The wrinkles may be formed by larger GO nanosheets protruding from the surface of the PEDOT matrix. The GO/PEDOT film morphology differs from that of conventional PEDOT films, which are characterized by small blister-like nodules at their surfaces (Figure S1) [31, 37]. The resulting nanocomposite film is a conductive, electrochemically stable electrode material. A comparison of the cyclic voltammogram (CV) of the bare GCE electrodes and the GO/PEDOT nanocomposite-modified electrodes demonstrated that the modified electrodes exhibit a much higher charge storage capacity, as indicated by the total area inside of the curve (Figure 1b). This property results from an increase in surface area as the nanocomposite film deposits on the surface of the electrode as well as an increased electroactivity contributed by PEDOT. Additionally, the electrochemical impedance of the electrode drops after modification with the nanocomposite, most notably in the lower frequency region (Figure 1c). In this low frequency range, impedances are influenced by the effective surface area of the electrode, with impedance value inversely correlating with surface area [38, 39]. A large effective surface area has implications for electrochemical sensing applications in which increased surface area may lead to an increased number of active sites for the targeted analyte and result in improved sensor properties.

Electrochemical detection of DA is often carried out *in vivo* by utilizing repeated CV scanning, during which the size of the DA oxidation peak is monitored over time to evaluate transient signaling in the central nervous system [8]. To evaluate its stability in response to repeated electrical stimulation, the nanocomposite-coated electrode underwent multiple CV scans and the electrochemical properties were monitored (Figure 1b, c). After two CV cycles, the low frequency impedance values slightly increased, suggesting that there was a minimal loss of surface area from the film, likely due to loosely adsorbed oligomers or GO nanosheets delaminating from the nanocomposite surface. As the electrode voltage is cycled during CV, the redox active PEDOT polymer switches between

its oxidized and reduced states and small ions or mobile dopant molecules move into and out of the polymer to neutralize the change in charge [40]. However, the large size of GO impedes its ability to exit the polymer during film reduction [33]. After 1000 CV cycles, there was no additional increase in the low frequency region, demonstrating reasonable electrical stability of the nanocomposite. GO nanosheets were undetectable with UV spectroscopy in PBS solutions in which the films were repeatedly CV cycled, supporting the stability of the nanosheets within the nanocomposite film. The shape of the CV curve, on the other hand, changed significantly and exhibited a decrease in the total charge storage capacity. Part of the decrease in charge storage capacity comes from a lower reduction current of PEDOT at -0.4 V, suggesting overoxidation of PEDOT, which may be avoided by sweeping the potential within a lower limit or increasing the scan rate.

3.2 Improved Sensitivity and Selectivity Toward DA Oxidation at the GO/PEDOT Nanocomposite

The electrochemical oxidation of DA, AA, and UA at the surface of the GO/PEDOT nanocomposite-modified electrodes was evaluated with CV and compared to the behavior of a bare GCE. Electrodes were assayed in solutions containing DA (100 μM), AA (1 mM) or UA (100 μM) separately, or in solutions containing all three analytes combined (Figure 2a, b). In the presence of all three analytes, the CV of the bare GCE exhibits only two distinguishable oxidation peaks, a result of the broad AA oxidation peak merging with the smaller DA oxidation peak. At the GO/PEDOT nanocomposite, DA exhibited a clear and separate oxidation peak (E_p = 147 mV) with no overlap from the interfering analyte oxidation peaks located at -28.6 mV for AA and at 287 mV for UA (Figure 2b). DA, AA, and UA coexist in the CNS and biological fluids such as cerebrospinal fluid and blood [8], making accurate quantification of the species difficult because of their close oxidation potentials. The GO/PEDOT-modified electrode enables more selective discrimination of DA than the bare GCE by increasing the separation between the oxidation peaks of DA and AA (Figure 2c). The increased separation arises from the significant leftward shift (E_p: 65.0 mV for bare GCE vs. -28.6 mV for GO/PEDOT, $p < 0.001$) and decreased width of the AA oxidation peak at the GO/PEDOT nanocomposite surface, that are likely a consequence of faster electron transfer to the film or improved electrocatalytic activity of the film towards AA oxidation [41, 42]. The ability of PEDOT modified electrodes to improve the separation of DA and AA by left-shifting the AA peak has been previously reported [13, 15]; however, the GO/PEDOT nanocomposite provides improved separation compared to conventional PEDOT films (Figure S2). Neither the DA nor UA molecules exhibit a change in their oxidation peak location and there is no effect on the separation between the two species at the GO/PEDOT nanocomposite surface compared to the bare GCE surface (Figure 2d). The absence of effect on the peak location indicates that the DA and UA oxidation reactions are not similarly electrocatalyzed by the GO/PEDOT film surface as is the AA oxidation reaction.

DA calibration curves of GO/PEDOT nanocomposite-modified electrodes and bare electrodes were compared to evaluate the sensitivity of the modified electrodes (Figure 2e). Within the range of 1 μM to 40 μM, the GO/PEDOT nanocomposite-modified electrode demonstrated a significant increase in sensitivity toward DA, indicated by the slope of the calibration curve (bare: 0.046 ± 0.005 μA μM^{-1}; GO/PEDOT: 0.151 ± 0.005 μA μM^{-1}; $p < 0.001$), with an improved accuracy, indicated by the linearity of the curve (bare: R^2 = 0.961; GO/PEDOT: R^2 = 0.995). The limit of detection, calculated assuming a signal-to-noise ratio of 3, was 83.0 nM for the GO/PEDOT electrode. The sensitivity of the GO/PEDOT material is comparable to that of conventional PEDOT (Figure S2) and composites consisting of CP and other carbon nanomaterials, such as carbon nanotubes, graphene or RGO, which have also demonstrated limits of detection in the nanomolar range [19, 26, 27, 43].

Carbon nanomaterials are noted for their unique physiochemical properties that have been implicated in improved biosensor performance [22, 44]. The sensitive detection of DA by the GO/PEDOT electrode may arise from a locally increased concentration of DA at the surface of the nanocomposite film as a result of interactions between the DA

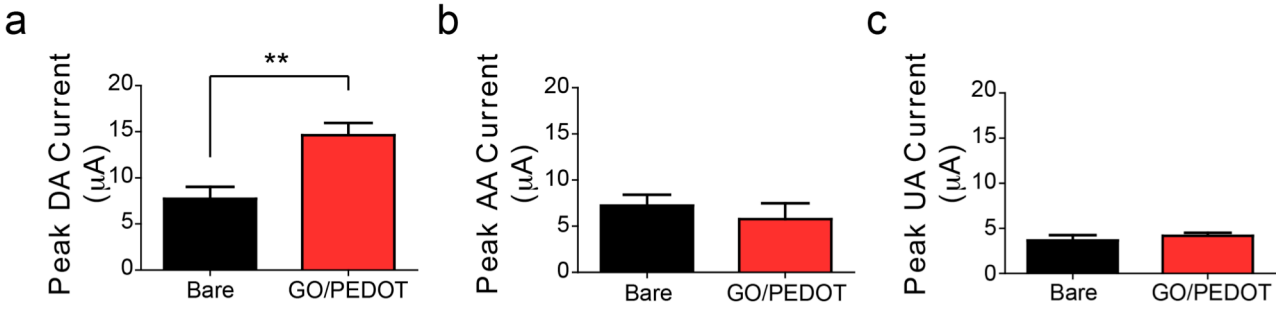

Figure 3: Selective Sensitivity of the GO/PEDOT Nanocomposite Towards DA. Peak oxidation current response of the bare and GO/PEDOT-modified electrodes in (a) 100 μM DA, (b) 1 mM AA, and (c) 100 μM UA measured by CV (100 mV s^{-1}). The GO/PEDOT nanocomposite selectively increases the DA oxidation current compared to the bare GCE, but not the AA or UA oxidation current (** $p < 0.01$; $n = 7$).

molecules and the nanocomposite surface. Notably, there is no improvement in sensitivity toward AA or UA at the GO/PEDOT nanocomposite, suggesting the mechanism of DA interaction is not shared by these molecules (Figure 3). At physiological pH, DA exists as a cation, while both AA and UA are anionic molecules. The difference in charge may play a role in the improved sensitivity *via* concentration of DA molecules at the nanocomposite surface through electrostatic interactions. While the bare GC electrodes contain some oxygen functional groups formed by polishing and electrochemical pretreatment that may impart a negative charge to the surface [45, 46], the GO/PEDOT nanocomposite contains a large amount of hydroxyl, carboxyl, and epoxide groups [31], with negatively-charged carboxyl groups located at the surface of the film that may electrostatically interact with DA [30]. While some of the negatively charged carboxyl groups are electrostatically interacting with the PEDOT backbone during the nanocomposite synthesis, the remaining carboxylic acid groups from GO impart to the nanocomposite film a net negative charge [47]. Along with electrostatic interactions between the anionic GO/PEDOT nanocomposite and the cationic DA molecules, π-π interactions may also play a role in the improved sensitivity toward DA. The DA molecule, but neither the AA nor UA molecule, contains a phenol ring that may readily participate in noncovalent π-π stacking with the benzene rings present in GO [48, 49].

3.3 Mechanisms Behind Improved DA Sensitivity of the GO/PEDOT Nanocomposite

The GO nanosheets within the nanocomposite provide a unique way to subtly alter its physical properties. By changing the size and shape of the GO nanosheets prior to deposition in the nanocomposite, the physical and chemical properties can be controllably altered without grossly changing the composition of the nanocomposite. Utilizing this unique property, the mechanism by which GO nanosheets contribute to the improved sensitivity to DA can be explored. True GO nanoparticles exist as two-dimensional, single-layer nanosheets (ca. 1 nm thickness), ranging in size in the x-y-direction from hundreds of nanometers to microns, depending on the extent of oxidation. However, during synthesis from graphite via the modified Hummer's method, many-layered GO platelets are formed as an intermediate to single-layer GO [47]. The GO platelets will persist until exfoliated by mechanical perturbation using sonication into single-layer GO, double-layer GO, and few-layer GO (3-10 nanosheet layers). With increasing sonication treatments, the distribution of sheet thicknesses shifts toward smaller values and the diameter of the sheets decreases [33, 50]. The size and thickness of the GO nanosheets can significantly alter the physical and chemical properties of the prepared GO/PEDOT nanocomposite without significantly changing its material composition, creating a unique method of probing the properties driving the electrochemical detection performance.

3.3.1 Effect of GO Sonication on the Nanocomposite DA Sensitivity and Chemical Properties

To investigate the effect of GO sonication on the properties of the GO/PEDOT nanocomposite, GO suspensions were sonicated for 15 min, 30 min, 60 min and 90 min prior to deposition into the nanocomposite. As the GO suspensions received longer sonication treatment, the average nanosheet thickness decreased (Figure S3). Electrodes modified with the sonication-treated GO/PEDOT nanocomposite were assayed for their sensitivity toward 100 μM DA using CV analysis in PBS. The magnitude of the peak DA oxidation current increased with increasing GO sonication treatment, with the 30 min, 60 min and 90 min treatment groups exhibiting a significantly larger peak current than a bare, unmodified electrode (Figure 4a; $p < 0.05$). The chemical composition of the nanocomposite films was evaluated using EDS to investigate the source of the improved sensitivity toward DA. The oxygen to sulfur (O/S) ratio provides a semi-quantitative measure of the amount of GO incorporated into the nanocomposite film. Each PEDOT unit contains a fixed O/S ratio (2:1), and the sulfur is present only in

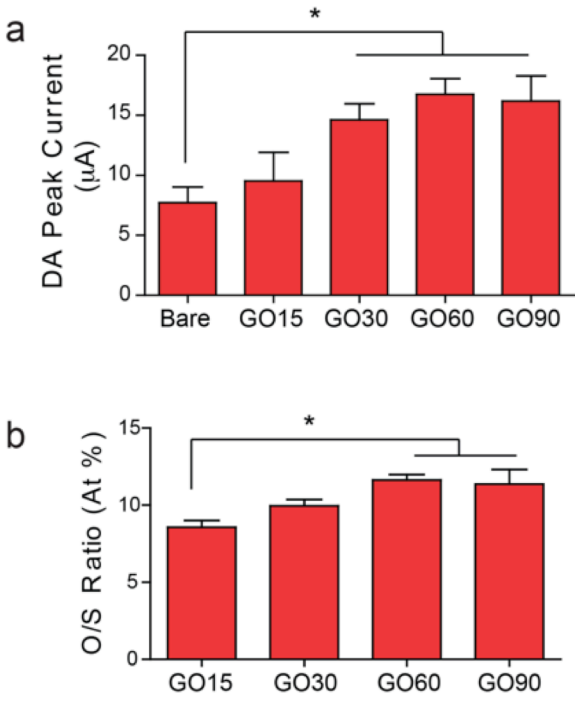

Figure 4. GO Sonication Improves Sensitivity of the GO/PEDOT Nanocomposite Towards DA. (a) Peak DA oxidation current in response to 100 μM DA at the bare GC electrodes and the GO/PEDOT nanocomposite synthesized with GO sonicated for 15 min (GO15), 30 min (GO30), 60 min (GO60), or 90 min (GO90) prior to electrodeposition into the composite (* $p < 0.05$; $n = 7$). (b) Atomic ratio of O to S in the nanocomposite synthesized from GO with varying sonication treatment prior to electrodeposition (* $p < 0.05$; $n = 5$). O/S ratio indicates the density of oxygen containing functional groups, donated by GO, in the nanocomposite film.

the polymer, not the GO nanosheets. As such, any increase in the O/S ratio indicates that there are 1) more GO sheets incorporated into the film, or 2) GO sheets with higher oxygen content selectively incorporated into the film. With increasing sonication treatment, the O/S ratio of the nanocomposite film increases significantly (Figure 4b; $p < 0.05$). It is most likely that the increased oxygen content arises from a larger number of GO nanosheets incorporating into the film. With sonication, the GO nanosheets decrease in size, and smaller molecules act as more efficient dopants in the electropolymerization reaction that creates the nanocomposite film [51].

The increased O/S ratio positively correlates to the magnitude of the DA oxidation current ($R^2 = 0.963$, $p < 0.05$), suggesting that the increased amount of GO nanosheets within the film may produce the improved sensitivity toward DA. GO nanosheets contain negatively charged carboxylic acid groups at its edges that may electrostatically interact with DA, and benzene rings within its plane that may interact with the phenol ring of DA via π-π interaction. To evaluate which type of interaction causes the improved sensitivity of the GO/PEDOT nanocomposite, CV analysis of 100 μM DA was carried out in PBS at pH 9.5. At this more basic pH, the amine group on the DA molecule is deprotonated (pKa: 8.9), rendering the molecule either neutral, or slightly negative, as the hydroxyl groups become deprotonated [52]. Additionally, at this higher pH, the GO/PEDOT nanocomposite film should become more negative as the pH moves further from the pKa of the carboxylic acid groups of the GO nanosheets [53]. At these conditions, there should be much less electrostatic interaction and possibly some electrorepulsion. As expected, the peak DA oxidation current at pH 9.5 (Figure 5a) is less than the current at physiological pH (Figure 4a) with a significant difference appearing for the nanocomposite film synthesized with GO receiving the 90-minute sonication treatment (pH 7.4: 16.18 μA; pH 9.5: 7.00 μA; $p < 0.01$). Additionally, the sonication effect present in physiological pH 7.4 conditions, in which the peak current increases with increased sonication time, is not exhibited at pH 9.5, and no differences arise between the electrode groups at the higher pH ($p = 0.1445$). These data support the hypothesis that the improved DA sensitivity demonstrated by the GO/PEDOT nanocomposite-modified electrodes at physiological pH is driven by electrostatic interactions between the positively charged amine group present on the DA molecules and the negatively charged carboxylic acid groups provided by the GO nanosheets in the GO/PEDOT nanocomposite. While π-interactions may exist between the benzene rings in the GO nanosheets and the phenol ring structure of the DA molecules, these interactions are clearly not the driving force behind the improved nanocomposite sensitivity that appears at higher GO sonication times because this effect completely disappears at the higher pH where the π-interactions would still persist.

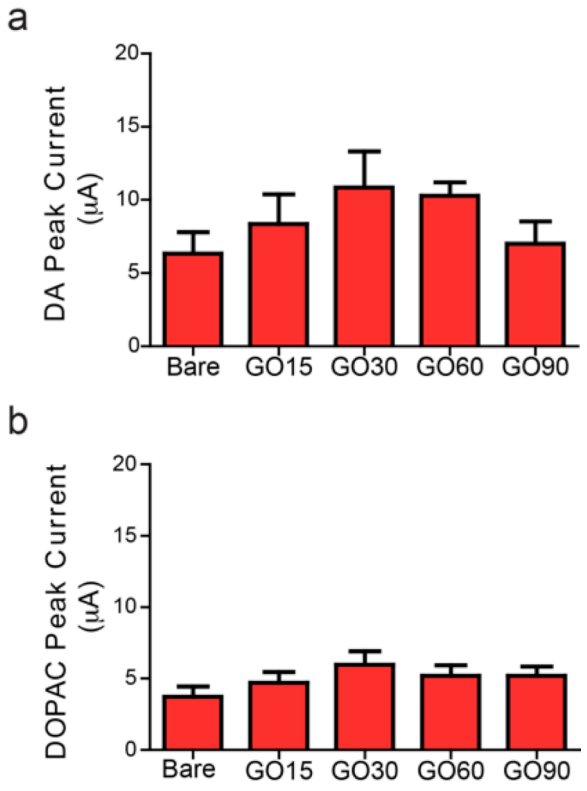

Figure 5. GO Sonication Does Not Effect Sensitivity of GO/PEDOT Nanocomposite Toward Neutral or Negatively Charged Analytes. (a) Peak DA oxidation current in response to 100 μM DA in PBS at pH 9.5 recorded at bare GCE and electrodes modified with the GO/PEDOT nanocomposite synthesized with GO sonicated for 15 min (GO15), 30 min (GO30), 60 min (GO60) or 90 min (GO90) prior to electrodeposition into the nanocomposite ($n = 7$). (b) Peak DOPAC oxidation current in response to 100 μM DOPAC in PBS at pH 7 recorded at bare GCE and electrodes modified with the nanocomposite synthesized from GO sonicated for varying amounts of time prior to deposition ($n = 7$).

To further confirm that electrostatic interactions play a role in the improved DA sensitivity of the GO/PEDOT nanocomposite, the electrochemical oxidation of DOPAC at the surface of the nanocomposite-modified electrodes was investigated with CV in PBS at physiological pH 7.4. DOPAC is a metabolite of DA and shares a similar structure to its precursor, with the exception that the amine group of DA is replaced with a carboxylic acid group to form the DOPAC molecule. At physiological pH, the DOPAC molecules exist as anions but retain the phenol ring structure. As such, the electrochemical oxidation behavior of DOPAC at the surface of the GO/PEDOT nanocomposite provides valuable information regarding the influence of electrostatic interactions vs. π-interactions on the sensitivity of the nanocomposite. At the surface of nanocomposite films synthesized with GO sonicated for 30 minutes or greater, the DOPAC peak oxidation current was significantly lower than the DA peak oxidation current ($p < 0.01$), demonstrating that the nanocomposite exhibits less sensitivity toward the DOPAC molecules. There is no influence of sonication treatment on the nanocomposite sensitivity toward DOPAC (Figure 5b), as was exhibited toward DA, suggesting that the source of interaction between DA and the

nanocomposite does not exist between DOPAC and the nanocomposite. The structure of DA and DOPAC are identical with the exception of their charged functional groups, confirming that electrostatic interactions between the DA amine and the GO carboxylic acid are likely the driving force behind the nanocomposite sensitivity.

3.3.2 Effect of GO Sonication on the Nanocomposite Electrochemical Properties

The electrochemical properties of the GO/PEDOT nanocomposite film synthesized with sonicated GO nanosheets were evaluated with electrochemical impedance spectroscopy to further probe the mechanism behind the improved electrochemical DA detection properties. The Nyquist plots of the nanocomposite impedance demonstrate characteristic behavior of GO-doped CP nanocomposites (Figure 6a) [30, 31, 34]. At low frequencies, the Nyquist plots exhibit steep slopes, indicative of highly capacitive behavior, while at high frequencies (Figure 6a inset) the curves present a more gradual slope that reflects the diffusive behavior of the film [34, 54]. Notably, the 15-minute sonication treatment group transitions from diffusive to capacitive behavior at a lower frequency than the other treatment groups; that is, it exhibits more diffusion-dominated behavior, indicating that the shorter sonication treatment may result in a nanocomposite film with slower charge transfer kinetics. The increase in diffusive behavior of the 15-minute sonication group may arise from a larger content of few-layer GO in the nanocomposite compared to longer sonication times that would contain more single- or double-layer GO. Inherently, GO is not conductive, a result of the disruption in its π-electron network as oxygen functional groups are added to the structure during its oxidation reaction [47]. Any larger GO nanosheets contained in the nanocomposite could decrease the charge transfer of the nanocomposite film or create a diffusion barrier at the electrode/electrolyte interface that would result in the observed Nyquist behavior.

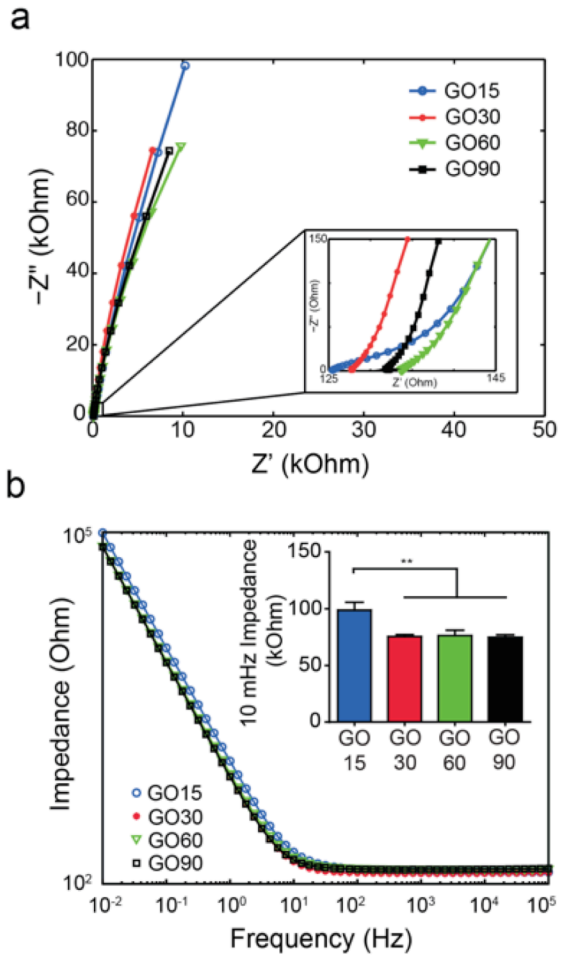

Figure 6. Effect of GO Sonication on the Electrochemical Impedence Spectroscopic Behavior of GO/PEDOT Nanocomposite. (a) Nyquist plots of the GO/PEDOT nanocomposites synthesized from GO sonicated for 15 min (GO15), 30 min (GO30), 60 min (GO60), or 90 min (GO90) prior to electrodeposition. Inset: High frequency range of the Nyquist plot displaying the increased diffusive behavior of the GO15 nanocomposite (n = 7). (b) Bode plots of the GO/PEDOT nanocomposites synthesized with GO sonicated for varying amounts of time prior to electrodeposition. Inset: Comparison of the 10 mHz impedance behavior (** $p < 0.01$; n = 7). The GO15 nanocomposite demonstrates significantly higher 10 mHz impedance, suggesting that it has a smaller effective surface area.

The impedance modulus of the nanocomposite films differs subtly as a result of GO sonication treatment (Figure 6b). At high frequencies, no significant changes emerge, but at impedances lower than approximately 10 Hz, the 15-minute sonication group diverges from the longer sonication groups. At the 10 mHz frequency, the impedance is significantly larger for the 15-minute sonication group than the longer sonication treatment groups ($p < 0.01$) indicating that the electrochemical surface area is smaller (Figure 6b inset) [38, 39]. The decreased surface area has implications for the sensitivity of the nanocomposite towards DA electrochemical oxidation, with a lower surface area likely to produce a decreased DA sensitivity. In fact, the 15-minute sonication group does display a lower DA oxidation peak current than the longer sonication groups, with no significant improvement over the bare electrode that exists for the longer treatments (Figure 4a). The difference in nanocomposite surface area likely arises from the fact that the sonication treatment alters the size of the GO nanosheets, with longer sonication creating smaller, thinner sheets. Increasing GO sonication treatment prior to electrodeposition into CP films results in a rougher nanocomposite topography and the appearance of smaller features at the surface, likely due to the fact that more small GO nanosheets are preferentially incorporated into the polymer matrix as dopants [33]. A rougher surface topography would possibly provide an increased number of active sites with which the DA molecules could electrostatically interact, improving the sensitivity of the nanocomposite film towards the electrochemical oxidation of DA. The increase in surface area supports the finding that increased oxygen content in the nanocomposite correlates to a higher sensitivity towards the electrochemical oxidation DA.

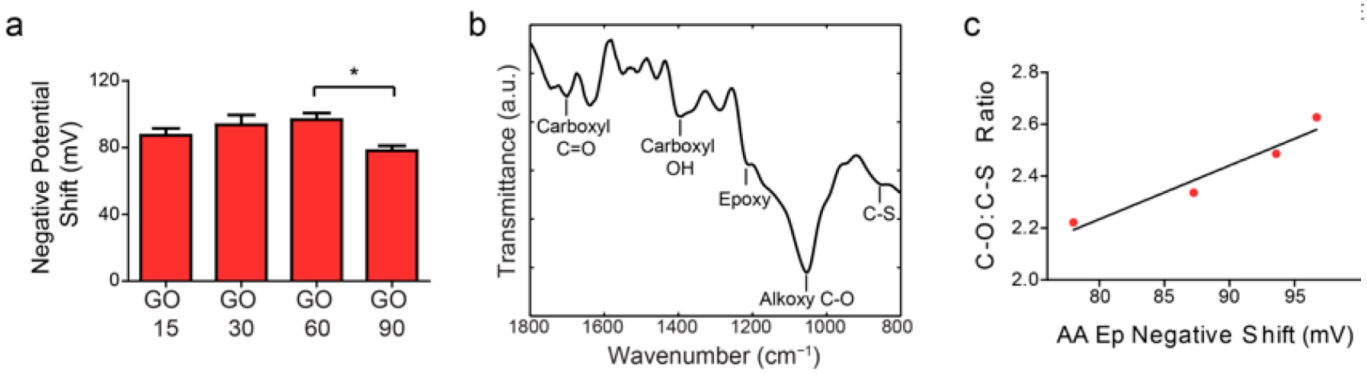

Figure 7: Alkoxy C-O Content in the GO/PEDOT Nanocomposite Correlates to the Shift in AA Oxidation Potential. (a) Negative shift in the AA oxidation potential, compared to a bare GC electrode, at the GO/PEDOT nanocomposite synthesized from GO sonicated for 15 min (GO15), 30 min (GO30), 60 min (GO60), or 90 min (GO90). The GO90 nanocomposite exhibits a significant decrease in the magnitude of AA oxidation potential shift (* $p < 0.05$; $n = 7$). (b) Representative FTIR spectrum of the GO90 nanocomposite exhibiting peaks corresponding to oxygen containing functional groups donated by the GO and the peak corresponding to the sulfur group donated by PEDOT. (c) Linear correlation between the magnitude of the AA oxidation potential (Ep) negative shift and the ratio of alkoxy C-O to C-S peaks. The ratio is a semi-quantitative estimate of the alkoxy content in the nanocomposites.

As more GO nanosheets are incorporated into the nanocomposite to increase its roughness and surface area, it is expected that there would be more carboxylic acid groups provided by the GO within the nanocomposite that would interact with DA molecules to produce the boosted sensitivity.

3.4 Effect of GO Sonication on the Electrocatalytic Activity Towards AA

At the surface of the GO/PEDOT nanocomposite, AA exhibits a leftward shift in its oxidation potential, demonstrating the electrocatalytic effect of the nanocomposite and its potential as a material to improve the specificity of electrochemical detection methods (Figure 2b, c). To probe the mechanism by which the nanocomposite interacts with AA, GO/PEDOT films were synthesized using GO that underwent graded sonication treatment and the effect on electrocatalysis of AA was evaluated. The negative shift in AA oxidation potential at the nanocomposite surface, as compared to a bare electrode, was significantly less at the longest sonication time of 90 min (Figure 7a). GO has been noted as a highly catalytic material because of the abundance of oxygen functional groups in its structure [55-57]. The electrocatalysis of the AA oxidation reaction by GO relies on the extent of GO oxidation, with higher levels of oxygen content correlating with increased electrocatalytic activity [58]. Interestingly, the favorable electrocatalysis has been shown to disappear when GO is chemically reduced, with the AA oxidation potential moving back towards the same positive voltage exhibited by the bare electrodes [58]. This suggests that the ability of GO to electrocatalyze the AA reaction lies with its readily reducible oxygen functional groups, such as hydroxyl or epoxide, but not its carbonyl groups that can persist in higher proportion following reduction [59, 60]. To explore the role of GO oxygen functional groups, the relationship between negative potential shift and oxygen bonds in the nanocomposite films was evaluated using FTIR (Figure 7b). The negative potential shift significantly correlated with the alkoxy C-O content in the nanocomposite ($R^2 = 0.967$, $p < 0.05$), but not to the other oxygen functional group content in the nanocomposite, suggesting that the electrocatalysis may arise from interactions between the AA molecule and the alkoxy functional groups present at the surface of the nanocomposite (Figure 7c). The AA electrochemical oxidation pathway is a two-step process with AA first directly oxidized into a dehydroascorbic acid (DHA) radical that adsorbs onto the electrode surface before further oxidation into the final product, DHA, which then desorbs from the electrode [61-63]. The formation of hydrogen bonds between the multiple hydroxyl groups on the DHA radical and the alkoxy groups of the GO nanosheets may be one way in which the nanocomposite catalyzes the oxidation reaction. The hydrogen bond interactions could coordinate the unstable DHA radical to reduce the energy barrier needed to carry out the reaction, resulting in a leftward shift in oxidation potential. At the longest sonication times, there is a reduction in available alkoxy groups, and a consequent reduction in the amount of hydrogen bond-mediated stabilization of the DHA radical would reduce the leftward shift observed in the AA oxidation potential as the reduction in the energy barrier to complete the reaction is not as large.

The origin of the decrease in alkoxy groups at the 90-min GO sonication time may be attributed to a population of smaller GO nanosheets, with a lower oxygen content per nanosheet, being incorporated into the nanocomposite. As the GO nanosheets are broken into smaller pieces with sonication treatment, only those that contain a negatively charged carboxylic acid group will be able to act as dopants in the electropolymerization reaction of the nanocomposite. Therefore, as smaller nanosheet sizes are produced at the longest sonication time, it is likely that the ratio of carboxylic acid to alkoxy in the nanocomposite would increase, and total alkoxy content would decrease, as small GO nanosheets containing only hydroxyl and epoxide groups are selectively omitted from the nanocomposite.

Notably, at the nanocomposite surface there is no change in the location of the oxidation potential for either DA or UA (Figure 2). The structure of DA contains fewer hydroxyl groups than the AA structure, and the UA molecule contains no hydroxyl groups. If stabilization of the intermediate radicals through hydrogen bonding with the alkoxy functional groups in the nanocomposite film drives the shift in the oxidation potential, the decreased number of opportunities for hydrogen bonding in the DA and UA molecules would potentially decrease the ability of the nanocomposite to catalyze their oxidation reactions in this manner. This selective electrocatalysis of the oxidation reaction of AA, but not DA, makes the GO/PEDOT nanocomposite a promising electrode material for the selective determination of DA in biological solutions that also contain AA, such as blood, urine, or cerebral spinal fluid.

4. Conclusions

The electrochemical oxidation behavior of DA, AA, and UA was investigated at the surface of a GO/PEDOT nanocomposite material. The nanocomposite selectively amplified the signal of DA oxidation as a result of electrostatic interactions between the DA molecules and the negative charges at the nanocomposite surface. Interference from AA was eliminated through electrocatalysis of the AA oxidation reaction by the nanocomposite surface, shifting its oxidation potential sufficiently away from the DA oxidation potential. These data indicate that this high performance nanocomposite material will be useful for the development of more selective and sensitive biosensors that will have the potential to improve both diagnostics and exploratory science by providing a more reliable and accurate depiction of DA in biological samples and tissues.

Acknowledgements

This work was supported by funding from the National Science Foundation grants 0748001, ERC-0812348 and DGE-0549352. C.L.W. acknowledges support from the University of Pittsburgh Provost's Development Fund. X.L. acknowledges the support of the Taishan Scholar Program of Shandong Province, China. The authors would like to thank the Nanoscale Fabrication and Characterization Facility at the University of Pittsburgh for access to material characterization instrumentation, the Center for Biological Imaging at the University of Pittsburgh for access to the scanning electron microscope, and T.D.Y. Kozai and N.R. Snyder for helpful discussions during the preparation of this manuscript.

Notes and references

[a] Department of Bioengineering, University of Pittsburgh, Pittsburgh, PA 15260, USA.
[b] McGowan Institute of Regenerative Medicine, University of Pittsburgh, Pittsburgh, PA 15260, USA.
[c] Center for the Neural Basis of Cognition, University of Pittsburgh, Pittsburgh, PA 15260, USA.
[d] College of Chemistry and Molecular Engineering, Qingdao University of Science and Technology, Qingdao 266042, P.R., China.

1. R.A. Wise, *Nat. Rev. Neurosci*., 2004, **5**, 483.
2. J. Lotharius and P. Brundin, *Nat. Rev. Neurosci.*, 2002, **3**, 932.
3. C.R. Yang, J.K. Seamans and N. Gorelova, *Neuropsychopharmacol.,* 1999, **21**, 161.
4. N.D. Volkow, J.S. Fowler, G.J. Wang and J.M. Swanson, *Mol. Psychiatr.*, 2004, **9**, 557.
5. C. Noelker, H. Hampel and R. Dodel, *Mol. Diagn. Ther.*, 2011, **15**, 83.
6. G. Eisenhofer, A.S. Tischler and R.R. de Krijger, *Endocr. Pathol*., 2012, **23**, 4.
7. J. Bicker, A. Fortuna, G. Alves and A. Falcao, *Anal. Chim. Acta*., 2013, **768**, 12.
8. D.L. Robinson, A. Hermans, A.T. Seipel and R.M. Wightman, *Chem. Rev*., 2008, **108**, 2554.
9. N.S. Lee, Y.Z. Hsieh, R.F. Paisley and M.D. Morris, *Anal. Chem*., 1988, **60**, 442.
10. D. Liu, Z. Wang and X. Jiang, *Nanoscale*, 2011, **3**, 1421.
11. B.H. Westerink, *J. Chromatogr. B*, 2000,**747**, 21.
12. R.J. Wickham, W. Solecki, L.R. Rathbun, N.M. Neugebauer, R.M. Wightman and N.A. Addy, *Front. Biosci.*, 2013, **5**, 982.
13. S.S. Kumar, J. Mathiyarasu, K.L.N. Phani and V. Yegnaraman, *J Solid State Electr.,* 2006, **10**, 13.
14. P.R. Roy, T. Okajima and T. Ohsaka, *Bioelectrochem*, 2003, **59**, 11.
15. V.S. Vasantha and S.M. Chen, *J Electroanal Chem*, 2006, **592**, 77.
16. M. Gerard, A. Chaubey and B.D. Malhotra, *Biosens. Bioelectron*., 2002, **17**, 345.
17. C. Janaky and C. Visy, *Anal. Bioanal. Chem*., 2013, *405*, 3489.
18. N. Rozlosnik, *Anal. Bioanal. Chem*., 2009, **395**, 637.
19. G.Y. Xu, B.B. Li, X.T. Cui, L.Y. Ling and X.L. Luo, *Sens. Actuat. B-Chem*. 2013, **188**, 405.
20. L. Zhang, Y. Wen, Y. Yao, J. Xu, X. Duan and G. Zhang, *Electrochim. Acta*, 2014, **116**, 343.
21. T. Kuila, S. Bose, P. Khanra, A.K. Mishra, N.H. Kim and J.H. Lee, *Biosens. Bioelectron.,* 2011, **26**, 4637.
22. Y. Liu, X. Dong and P. Chen, *Chem. Soc. Rev*., 2012, **41**, 2283.
23. L. Tang, Y. Wang, Y. Li, H. Feng, J. Lu and J. Li, *Adv. Funct. Mater*., 2009, **19**, 2782.
24. M. Zhou, Y.M. Zhai and S.J. Dong, *Anal. Chem*., 2009, **81**, 5603.
25. J. Li, J. Yang, Z.J. Yang, Y.F. Li, S.H. Yu, Q. Xu and X.Y. Hu, *Anal. Methods-UK*., 2012, **4**, 1725.
26. P. Si, H.L. Chen, P. Kannan and D.H. Kim, *Analyst*, 2011, **136**, 5134.
27. W. Wang, G. Xu, X.T. Cui, G. Sheng and X. Luo, *Biosens. Bioelectron.,* 2014, **58C**, 153.
28. X. Zhu, Q. Liu, X.H. Zhu, C.L. Li, M.T. Xu and Y. Liang, *Int. J. Electrochem. Sc*., 2012, **7**, 5172.
29. M. Deng, X. Yang, M. Silke, W.M. Qiu, M.S. Xu, G. Borghs and H.Z. Chen, *Sensor. Actuat. B-Chem*., 2011, **158**, 176.
30. X. Luo, C.L. Weaver, S. Tan and X.T. Cui, *J .Mater. Chem. B*, 2013, **1**, 1340.
31. A. Osterholm, T. Lindfors, J. Kauppila, P. Damlin and C. Kvarnstrom, *Electrochim. Acta*, 2012, **83**, 463.
32. H. Tian, J. Liu, D. Wei, X. Kang, C. Zhang, J. Du, B. Yang, X. Chen, H. Zhu, Y. NuLi and C. Yang, *Biomaterials*, 2013, **35**, 2120.

33. C.L. Weaver, J.M. LaRosa, X. Luo and X.T. Cui, *ACS Nano*, 2014, **8**, 1834.
34. C.Z. Zhu, J.F. Zhai, D. Wen and S.J. Dong, *J. Mater. Chem*., 2012, **22**, 6300.
35. W.S. Hummers and R.E. Offeman, *J. Am. Chem. Soc*., 1958, **80**, 1339.
36. S. Agarwal, X. Zhou, F. Ye, Q. He, G.C. Chen, J. Soo, F. Boey, H. Zhang and P. Chen, *Langmuir*, 2010, **26**, 2244.
37. X.T. Cui and D.D. Zhou, *IEEE-EMBS*, 2007, **15**, 502.
38. Y.Y. Duan, G.M. Clark, R.S.C. Cowan, *Proc. SPIE*, 2001, **4235**, 498.
39. F.B. Karp, N.A. Bemotski, T.I. Valdes, K.F. Bohringer and B.D. Ratner, *IEEE Sens. J*., 2008, **8**, 104.
40. G.G. Wallace, Conductive Electroactive Polymers : Intelligent Polymer Systems. 3rd ed, Boca Raton, CRC Press, 2009.
41. M.R. Deakin, P.M. Kovach, K.J. Stutts and R.M. Wightman, *Anal. Chem*., 1986, **58**, 1474.
42. R.A. Saraceno, J.G. Pack and A.G. Ewing, *J. Electroanal. Chem*., 1986, **197**, 265.
43. Z.J. Zhuang, J.Y. Li, R.A. Xu and D. Xiao, *Int. J. Electrochem. Sc*. 2011, **6**, 2149.
44. N. Sinha, J.Z. Ma and J.T.W. Yeow, *J. Nanosci Nanotechnol*., 2006, **6**, 573.
45. R.C. Engstrom and V.A. Strasser, *Anal. Chem*., 1984, **56**, 136.
46. I.F. Hu, D.H. Karweik and T. Kuwana, *J. Electroanal. Chem*., 1985, **188**, 59.
47. D.R. Dreyer, S. Park, C.W. Bielawski and R.S. Ruoff, *Chem. Soc. Rev*., 2010, **39**, 228.
48. M. Bagherzadeh and M. Heydari, *Analyst*, 2013, **138**, 6044.
49. A. Rochefort and J.D. Wuest, *Langmuir*, 2009, **25**, 210.
50. J. Russier, E. Treossi, A. Scarsi, F. Perrozzi, H. Dumortier, L. Ottaviano, M. Meneghetti, V. Palermo and A. Bianco, *Nanoscale*, 2013, **5**, 11234.
51. T.V. Vernitskaya and O.N. Efimov, *Russ. Chem. Rev*., 1997, **66**, 489.
52. J. Armstrong and R.B. Barlow, *British J. Pharmacol*., 1976, **57**, 501.
53. B. Konkena and S. Vasudevan, *J. Phys. Chem. Lett*., 2012, **3**, 867.
54. C. Peng, J. Jin and G.Z. Chen, *Electrochim. Acta*, 2007, **53**, 525.
55. D.R. Dreyer, H.P. Jia and C.W. Bielawski, *Angew. Chem. Int. Edit*., 2010, **49**, 6813.
56. J. Pyun, *Angew. Chem. Int. Edit*., 2011, **50**, 46.
57. A. Dhakshinamoorthy, M. Alvaro, P. Concepcion, V. Fornes and H. Garcia, *Chem. Commun*., 2012, **48**, 5443.
58. D.V. Stergiou, E.K. Diamanti, D. Gournis and M.I. Prodromidis, *Electrochem. Commun*., 2010, **12**, 1307.
59. A. Bagri, C. Mattevi, M. Acik, Y.J. Chabal, M. Chhowalla and V.B. Shenoy, *Nat. Chem*., 2010, **2**, 581.
60. W. Gao, L.B. Alemany, L.J. Ci and P.M. Ajayan, *Nat. Chem*., 2009, **1**, 403.
61. M. Brezina, J. Koryta, T. Loucka and D. Marsikova, *J. Electroanal. Chem*., 1972, **40**, 13.
62. P. Karabinas and D. Jannakoudakis, *J. Electroanal. Chem*., 1984, **160**, 159.
63. M. Rueda and A. Aldaz, *Electrochim. Acta*, 1978, **23**, 419.